PRELIMINARY ANALYSIS OF DYNAMIC STALL EFFECTS
ON A 91-METER WIND TURBINE ROTOR

Robert E. Wilson

Oregon State University
Corvallis, Oregon 97331

ABSTRACT

Analytical investigation of dynamic stall on HAWT rotor loads was conducted. Dynamic stall was modeled using the Gormont approach on the MOD-2 rotor, treating the blade as a rigid body teetering about a fixed axis. Blade flapwise bending moments at station 370 were determined with and without dynamic stall for spatial variations in local wind speed due to wind shear and yaw. The predicted mean flapwise bending moments were found to be in good agreement with test results. Results obtained with and without dynamic stall showed no significant difference for the mean flapwise bending moment. The cyclic bending moments calculated with and without dynamic stall effects were substantially the same. None of the calculated cyclic loads reached the level of the cyclic loads measured on the MOD-2 using the Boeing five-minute-average technique.

NOMENCLATURE

a	Speed of sound
C_L	Lift coefficient
c	Blade chord
I	Teeter moment of inertia
M	Flapwise bending moment
M	Mach number
r	Distance along blade
R	Blade radius
s	Distance measured normal to axis of rotation
v	Blade of deflection
V	Wind speed
w	Aerodynamic load per unit span
W	Local relative velocity
$\dot{\alpha}$	Time rate of change of angle of attack
α	Angle of attack
γ_L	Dynamic stall parameter
δ	Yaw angle
δ_3	Teeter axis tilt
ψ	Teeter angle
μ	Blade mass per unit span
θ	Master blade position angle
Ω	Rotor angular velocity

INTRODUCTION

Large horizontal axis wind turbine rotors experience on the order of 10^9 stress cycles during a projected 30-year lifetime. Cyclic loads due to gravity, tower shadow, wind shear, and yaw contribute to stress cycling as well as wind turbulence which can be viewed as a cyclic disturbance in the reference system of the blade. With the exception of gravity, the loads mentioned above are aerodynamic in nature and, since dynamic stall has been identified as playing a significant role in influencing the performance and fatigue life of the vertical axis wind turbine [1], it has been conjectured that dynamic stall plays a similar role in influencing cyclic loads of horizontal axis wind turbines.

The primary characteristics of dynamic stall are the occurrence of stall beyond the angle of attack associated with the static stall, the dependence of the loads on the time rate of change of the angle of attack as well as the angle of attack, and hysteresis in the lift, drag, and pitching moment. These characteristics would be expected to increase both mean and cyclic loadings. Noll and Ham [2] in their investigation of the effects of dynamic stall on small wind systems concluded that dynamic stall could increase fixed pitch horizontal axis wind turbine normal loads and moments by "about 10 percent." Accordingly, this study was undertaken to examine the possible effects of dynamic stall on the MOD-2 wind turbine. Extensive data on mean and cyclic flapwise loads have been obtained for the MOD-2 [3].

ANALYSIS

Geometry

The analytical model used to investigate the effect of dynamic stall on the mean and cyclic flapwise bending moments consisted of a rigid two-bladed rotor teetering about a fixed point. An existing program [4] was modified to treat a teetering rotor. Figure 1 shows a blade element, the wind, V_W, and the coordinate system. Looking upwind, the rotation of the rotor is counterclockwise with the rotor teeter angle designated as ψ. The axis of rotation, x, is fixed in space so that rotor yaw, represented by the angle δ, is due to shifting of the wind rather than motion of the yaw axis. Each blade of the two-bladed rotor lies in the same plane so that there is no precone to the rotor.

The blade positions differ by an angle of 180° and the teeter angles of the two blades differ in algebraic sign. One blade is designated as the master blade and the position angle, θ, and the teeter angle, ψ, are given for the master blade.

Blade Bending Moment

The blade element illustrated in Figure 1 is shown in Figure 2 as part of a blade section which extends from r, to the blade tip. Loadings due to the aerodynamic forces and the centrifugal accelerations are illustrated in Figure 2. For a blade element of mass per unit span, μ, rotating at a constant angular velocity, Ω, the contribution of the above loadings on the element to the flatwise bending moment at position s, is

$$dM_1 = (s-s_1)(w-\mu\ddot{v})dr - \mu s\Omega^2(v-v_1)dr \qquad (1)$$

Here w is the aerodynamic load per unit span. Rigid body motion of the rotor blade due to teeter motion yields $v = r\sin\psi \approx r\psi$ so that the contribution to the flapwise bending moment becomes

$$dM_1 = (r-r_1)[w - \mu r(\ddot{\psi} + \Omega^2\psi)]dr \qquad (2)$$

The motion of the rotor about the teeter axis when ψ is small and the teeter axis is perpendicular to the blade span $(\delta_3 = 0)$ is described by

$$I(\ddot{\psi} + \Omega^2\psi) = M_{net} \qquad (3)$$

41

where

$$I = 2 \int_o^R r^2 \mu dr \qquad (4)$$

and the net teeter moment is

$$M_{net} = \int_{Blade\ 1} r w dr - \int_{Blade\ 2} r w dr$$

Substitution of Eq. (3) into Eq. (2) yields an expression for the differential flapwise contributions of the aerodynamic forces and the accelerations (both centrifugal and teetering) to the flapwise bending moment.

$$dM_1 = (r-r_1) w dr - \frac{M_{net}}{I} (r-r_1) r \mu dr \qquad (5)$$

Measurements of the flapwise bending moment of the MOD-2 wind turbine were made at station 370. At this station, the contributions given in Eq. (6) can be written as

$$M_1 \Big|_{aero} - 0.352\ M_{net}$$

Gravitational contributions must also be included. Including the blade twist at station 370 (twist = β = 2.5°) the bending moments due to gravity are

$$g \int_{r_1}^R (r-r_1) \mu dr\ [\sin\psi \cos\beta \sin\theta + \sin\beta \cos\theta] \qquad (6)$$

For the MOD-2 with small ψ the above contribution is

$$3,219,000\ \psi\sin\theta + 142,900\ \cos\theta\ \ N\text{-}m$$

The total of the gravitational, aerodynamic, and acceleration contributions to the flapwise bending moment at station 370 is

$$M_1 \Big|_{Total} = M_1 \Big|_{aero} - 0.352 M_{net} + 3.219 \cdot 10^6 \psi\sin\theta$$
$$+ 1.43 \cdot 10^5 \cos\theta \qquad (7)$$

The gravity terms play a large role in determining the cyclic bending moments.

Wind Input

The wind input used to model the effects of dynamic stall consisted of a steady wind with a yaw angle of 15° and with wind shear. The surface roughness used was 0.32 m which yields a peak wind speed of 1.107 V_{hub} when the blade tip is at its highest position and a minimum wind speed of 0.736 V_{hub} when the blade top is at its lowest position. Examination of Goldendale test site wind measurement records indicated that the mean shear corresponds to a surface roughness of 0.32 m. This surface roughness yields a wind profile that is close to a power law profile exponent of 0.2.

The yaw angle of 15° was selected after examination of the PG&E MOD-2 wind turbine data. It was observed that yaw angles of 15° were sustained for periods in excess of 30 seconds, which is the length of time

necessary for the MOD-2 rotor to fully respond to a step change in wind conditions. Both the wind shear and the yaw produce cyclic changes in the angle of attack. Wind shear changes the velocity component normal to the blades, while the yaw produces cyclic changes in the component of the relative velocity parallel to the blade. Thus, shear-induced changes in angle of attack are greatest at the blade tips while yaw cyclic angles of attack are greatest near the blade roots.

Aerodynamics

The aerodynamic forces on the blades were obtained from integration of the local forces obtained from strip theory. Equating the blade forces on a blade element to the momentum change in differential element, the induced axial velocity was calculated at each angular position at stations along the blade radius. The net aerodynamic moment causing the rotor to teeter was calculated and used to determine the teeter angular velocity. Integration of the teeter angular velocity, $\dot\psi$, yielded the teeter angle. The blade forces were determined using the velocity of the air relative to the blades so that the local teeter velocity, $r \cos\psi\dot\psi$, (the MOD-2 has no δ_3) played a significant role in determining the induced axial velocity of the air. The tangential induced velocity was neglected.

Strip theory uses the concept of a fully developed wake in the calculation of the induced axial velocity so that there is an implicit assumption that an equilibrium-wake exists. That is, the wake is always in equilibrium with conditions on the blade.

Static aerodynamic data for the NACA 23000 series airfoil used on the MOD-2 were obtained from reference [5]. No correction was included in the calculations for the gap between the movable tips and the fixed portion of the blade and the Prandtl tip loss factor was used to account for decay of the circulation at the blade tips.

Dynamic Stall Model

The Gormont approach [6] was selected to model the effects of dynamic stall based on the simplicity of the method and success in treating dynamic stall in vertical axis wind turbine applications [7]. In the Gormont method

$$C_L = \frac{C_L(\alpha_R)}{\alpha_R - \alpha_{L_o}} \alpha_{static} \qquad (8)$$

where

$$\alpha_R = \alpha_{static} - \gamma_L \sqrt{\left|\frac{c\dot\alpha}{2W}\right|}\ [.25 + .75 \frac{\dot\alpha}{|\dot\alpha|}] \qquad (9)$$

and γ_L is a dynamic stall parameter that depends upon the airfoil shape and Mach number. Since the MOD-2 blade varies considerably in thickness ratio along the span, varying from 12% thickness ratio at the tips to 27.2% thickness ratio at $r = 0.3R$, there was little data available on the parameter γ_L. Using extrapolation of the data given in Gormont's report [6], the following form of γ_L was obtained and used for this study:

$$\gamma_L = (2.66 - 6.98 \; t/c) \left[1 - \frac{M}{1.035 - 2.5 \; t/c}\right] \qquad (10)$$

Table 1 below gives the variation of γ_L over the MOD-2 blade using a local Mach number, $M = r\Omega/a$.

Table 1. Variation of γ_L with Radial Station

r/R	t/c	γ_L
1.00	.12	1.21
.85	.17	.98
.70	.22	.74
.50	.24	.68
.30	.27	.60

The extrapolation used to characterize the dynamic stall parameter does not warrant the display of two-digit accuracy shown in Table 1; the values are shown to indicate the magnitudes used in this study.

Cases Examined

The effect of dynamic stall on the mean flapwise and cyclic bending moments was examined at three wind speeds, 9, 11.5, and 14 m/s. Cases were run with and without dynamic stall. The calculations were started with the rotor in horizontal position with zero teeter angle and the history was determined for six revolutions. Calculations at 14 m/s were made for eight revolutions. The largest cyclic loads were obtained at the final revolution with no appreciable differences being observed between the sixth and eighth revolution. Integration increments of 0.05 R and 0.10 R were used and it was found that the smaller integration increment resulted in an 8.7% increase in mean flatwise bending moment and an increase of 0.8% in the cyclic bending moment.

The results reported are for the 0.10 R integration increment, the larger integration increment having a significant effect on the computation costs, approximately cutting the costs in half.

All the reported runs were made with fixed pitch of 2° on the partial span control surfaces. Interaction between the wind conditions and the control system was not included in this study.

RESULTS

The results obtained for the MOD-2 wind turbine are shown in Figures 3 and 4. Figure 3 shows the mean flapwise bending moment measured at the Goldendale, WA test site as a function of the mean wind speed measured at the BPA tower. Also shown in Figure 3 is the mean flapwise bending moment calculated in this study. There is good agreement between the calculated mean flapwise bending moment and the measured value. The mean flapwise bending moment is almost exclusively due to aerodynamic contributions since the net contribution from gravity and teeter is zero.

Figure 4 shows the cyclic flapwise bending moment data for Goldendale Unit #3. The data shown for 50% occurrence are based on measurements, and the 99.9% case is based on calculations using the 50% data.

The cyclic moments shown as the 50% occurrence were obtained by statistical analysis of the amplitudes of bending moment variations from the mean taken over many cycles. Another method of representing the

cyclic variations is to take the cyclic amplitude as $1/2 \; (M_{max} - M_{min})$ where M_{max} is the maximum value in a cyclic and M_{min} is the minimum value of the cycle. Table 2, shown below, gives the results in tabular form. Cyclic flapwise bendings calculated using the $1/2 \; (M_{max} - M_{min})$ method are given along with $(M_{max} - \tilde{M})$ and the test results. Using either approach, the calculated cyclic bending moment is below the measured value.

Dynamic stall for the cases considered is observed to have a small effect. At the lowest wind speed considered, 9 m/s, there was virtually no effect of dynamic stall, due to the fact that angles of attack were below static stall over most of the blade. As the wind velocity was increased, dynamic stall effects on the bending moment increase, but the magnitudes of these increases were modest. The results at 14 m/s show that dynamic stall increased the mean bending moment by 2.5% and the cyclic bending moment increased by 3.3% to 9.0% depending upon the method used to calculate the cyclic bending moment. Regardless of the method used to calculate the cyclic bending moment, the calculated values were less than the measured values at the cyclic bending moment obtained from reference [3].

Table 2. Calculated Mean and Cyclic Flapwise Bending Moments at Station 370

Wind Speed m/s	Dynamic Stall	$\tilde{M}$ N·m	$\frac{1}{2}(M_{max} - M_{min})$* N·m	$M_{max} - \tilde{M}$ N·m	ΔM_{cyclic}** (Data) N·m
9.0	No	$1929 \cdot 10^3$	172317	202730	
9.0	Yes	$1932 \cdot 10^3$	173656	205033	241000
11.5	No	$2455 \cdot 10^3$	193661	232386	
11.5	Yes	$2481 \cdot 10^3$	198066	248431	299000
14.0	No	$2848 \cdot 10^3$	229245	274480	
14.0	Yes	$2918 \cdot 10^3$	236758	299075	357000

* Plotted in Figure 3
**Cyclic flapwise bending moment data, 50% occurrence from Figure 4

CONCLUSIONS

The results obtained for cyclic and mean flapwise bending moment for cases with and without dynamic stall show no substantial change due to the inclusion of dynamic stall. Further comparisons of calculated and measured bending moments show good agreement for the mean bending moments and poor agreement for the cyclic bending moments. The cyclic bending moments calculated were for a 15° yaw angle which is a frequent, but not the usual, case for the MOD-2. It is concluded that spatial variations in wind speed due to wind shear and yaw are not the primary drivers of cyclic loading. Further, the effect of dynamic stall on the mean and cyclic bending moments is small. Wind turbulence and rotor flexibility were omitted in this preliminary study of the effects of dynamic stall and, of these omissions, wind turbulence is felt to play a significant role in determining the magnitude of the cyclic loads. The role of dynamic stall in interacting with wind turbulence remains unknown with the major barrier to understanding being the inclusion of wind turbulence in the loading analysis.

REFERENCES

1. Klimas, P.C., "Vertical Axis Wind Turbine Aerodynamic Performance Prediction Methods," Presented at Vertical Axis Wind Turbine (VAWT) Design Technology Seminar for Industry, sponsored by DOE and Sandia Laboratories, Albuquerque, NM, April 1-3, 1980.

2. Noll, R.B. and Ham, N.D., "Dynamic Stall of Small Wind Systems," Rockwell International Corporation, Energy Systems Group, Rocky Flats Plant, Report RFP-3523, UC-60, Golden, CO, Feb. 1983.

3. _____ "MOD-2 Wind Turbine System Development Final Report," Volume I - Executive Summary, Prepared by Boeing Engineering and Construction for NASA Lewis Research Center DOE/NASA/002-1, NASA CR-168006, Sep. 1982.

4. Wilson, R.E and Patton, E.M., "Design Analysis of Performance and Aerodynamic Loading of Rigid Rotor HAWT," RIO/2227-78/2, UC-60, OSU, Corvallis, OR, Aug. 1978.

5. Wilson, R.E. and Walker, S.N., "Performance Analysis of Horizontal Axis Wind Turbines," Draft Final Report, OSU, Corvallis, OR, Mar. 1984.

6. Gormont, R.E., "A Mathematical Model of Unsteady Aerodynamics and Radial Flow for Application to Helicopter Rotors," USAAMRDL, TR 72-67, May 1973.

7. Oler, J.W., Strickland, J.H., Im, B.J., and Graham, G.H., "Dynamic Stall Regulation of the Darrieus Turbine," Sandia National Laboratories Contractor Report SAND83-7029, Aug. 1983.

The following Appendices involve subjects of general interest to HAWT developers.

APPENDIX A

WAKE EXPANSION MODEL

A simple analytical model for the wake and flow field of a horizontal axis wind turbine can be developed from actuator disk theory. Let the mean axial velocity at the rotor by $u = V(1-\bar{a})$ and the mean axial velocity in the far wake by $u_{FW} = V(1-\lambda\bar{a})$. The axial velocity along the axis of a rotor is approximated by

$$v_x = V\left[1-\bar{a} - \bar{a}\,\frac{(\lambda-1)q}{\sqrt{1+q^2}}\right] \qquad (A-1)$$

where $q = x/R$, R is the rotor radius and the rotor is at the origin with x measured downstream. The above relation is exact for the velocity along the axis of a rotor with a cylindrical vortex sheet wake when $\lambda = 2$. Using the above equation for v_x throughout the flow field one obtains from the continuity equation

$$v_r = \frac{V\bar{a}(\lambda-1)\eta}{2\left(1+q^2\right)^{3/2}} , \qquad \eta \equiv \frac{r}{R} \qquad (A-2)$$

which yields a linear variation with r for the radial velocity, v_r. The linear variation in radial velocity is in qualitative agreement with the results of a free wake analysis.

Streamlines in the flow may be obtained from the relation:

$$\left(\frac{dr}{dx}\right)_{S.L.} = \left(\frac{d\eta}{dq}\right)_{S.L.} = \frac{v_r}{v_x} \qquad (A-3)$$

Integration of this equation yields

$$\frac{R_{wake}}{R} = \left(1 - \frac{Eq}{\sqrt{1+q^2}}\right)^{-1/2} \qquad (A-4)$$

where $E \equiv \bar{a}(\lambda-1)/(1-\bar{a})$. Equation (A-4) may also be used for any streamline that starts at the rotor.

In order to use the above approximation relation, values of $\bar{a}$ and λ are required. The value of $\bar{a}$ is a mean value of the induction at the rotor and can be approximated from the thrust coefficient.

For $C_T < 0.64$, $\lambda = 2$ and

$$C_T = 4\bar{a}\,(1-\bar{a}) \qquad (A-5)$$

which is a quadratic equation.

For $C_T > 0.64$

$$C_T = 0.16 + 2.4\bar{a} \qquad (A-6)$$

while λ can be obtained from

$$\lambda = \frac{C_T}{2\bar{a}(1-\bar{a})} \qquad (A-7)$$

The equation for the wake boundary is an approximation and although it satisfies continuity, Eq. (A-4) has positive curvature for the streamlines at the rotor. The point of zero curvature for the streamlines is defined by

$$E\left(q^2 + 5/6\right) = q\,\sqrt{1+q^2}$$

The point of zero streamline curvature varies from the rotor at E=0 (no wake expansion) to $q \doteq 1.42$ for E=1 (infinite wake diameter).

APPENDIX B

FREE YAW OF RIGID HUB ROTORS

The stability of rigid hub rotors in free yaw may be described by examination of the change in yaw moment with the yaw angle, δ.

$$k \equiv -\frac{\partial M_{yaw}}{\partial \delta} \qquad (B-1)$$

44

Other yaw moments can cause yaw tracking errors but the yaw stability is determined by magnitude and the algebraic sign of k. While yaw tracking errors are mostly due to the imbalance of in-plane aerodynamic forces due to wind shear and tower shadow, the spring constant, k, is due to the normal aerodynamic forces. Figure B-1 illustrates the role of the coning angle ψ in the stability of rigid hub rotors in free yaw.

A rotor with blade horizontal is shown schematically when viewed from above. The velocity normal to the blades is shown for blade elements on the right hand side and the left hand side of the rotor. The velocity normal to the blade determines the angle of attack; that is

$$\alpha \sim V_\perp \qquad (B-2)$$

The induction may be different on opposite sides of the rotor; however, the primary dependence is due to the normal velocity. It may be observed that

$$V_{\perp_R} > V_{\perp_L}$$

hence the angles of attack for the illustrated blade will obey

$$\alpha_R > \alpha_L \qquad (B-3)$$

for the illustrated figure.

The normal forces on the right hand and left hand sides are proportional to $\alpha\,C_{L_\alpha}$, hence the moment about point 0 tending to yaw the rotor in the δ-direction is proportional to

$$-C_{L_\alpha}\,(\alpha_R - \alpha_L) \qquad (B-4)$$

The spring constant, k, is the result of integration of the differential yaw moment due to yaw over the rotor. If $C_{L_\alpha} > 0$ the illustrated rotor will be stable in yaw since the coning angle ψ produces a greater normal force on the blade occupying the right hand side of the rotor than on the left. However, beyond stall for many airfoil sections, $C_{L_\alpha} < 0$, and the rotor yaw moment will increase with increasing yaw. In such a case the rotor will operate in stable mode at an upwind position where the coning angle is negative. Thus the stability of rigid rotors horizontal axis wind turbines in yaw can be characterized by the integrated contribution of $C_{L_\alpha}\,\psi$ over the rotor. For a rotor with three or more blades (B = number of blades) the dominant term in the yaw "spring constant" is

$$\frac{B}{2\pi} \int_0^1 \left(\frac{c}{R}\right) \eta^2 X\, C_{L_\alpha}\, \psi\cos\phi\, d\eta$$

where

$$\eta = r/R$$

$$X = \frac{R\Omega}{V}$$

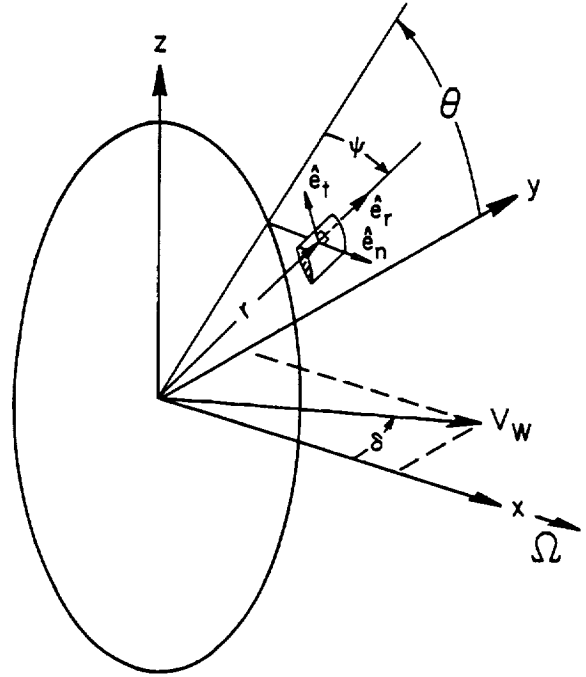ϕ is the local flow angle with respect to the rotor disk.

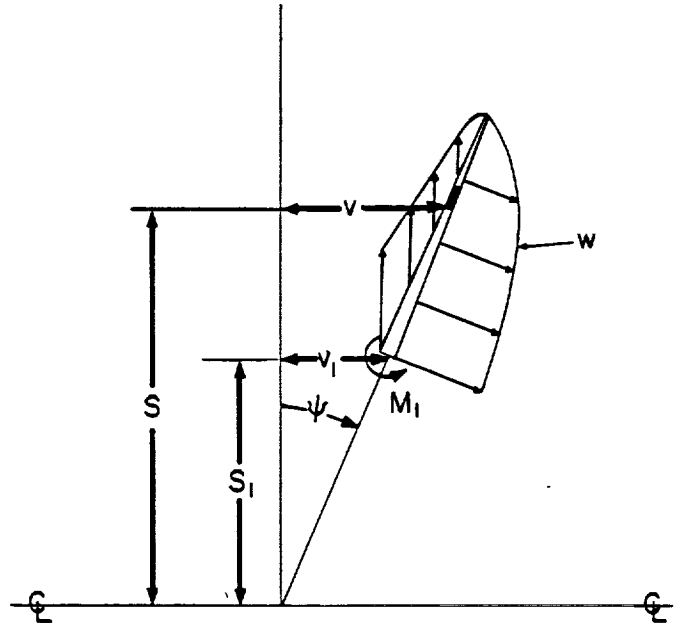Figure 1. Rotor Geometry and Coordinates

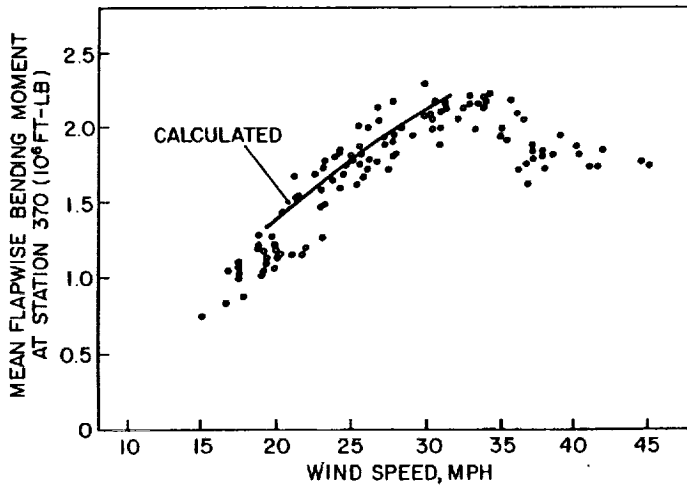Figure 2. Blade Section with Aerodynamic and Centrifugal Loading

45

Figure 3. Mean Flapwise Bending Moment at Station
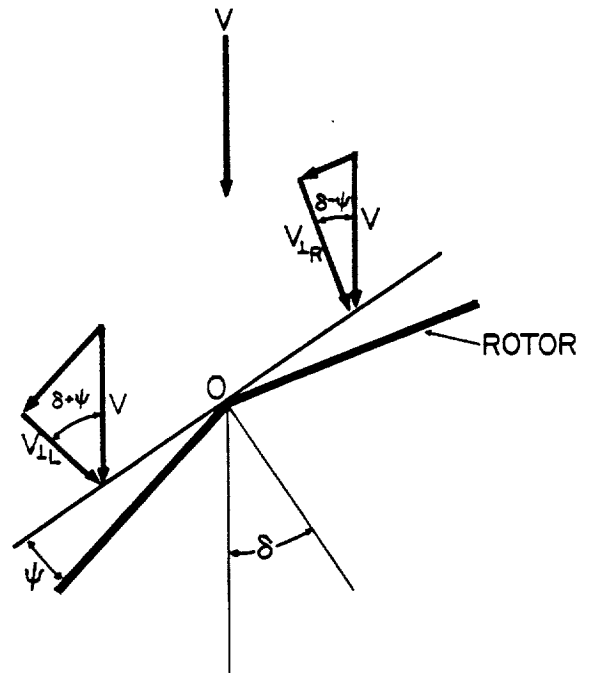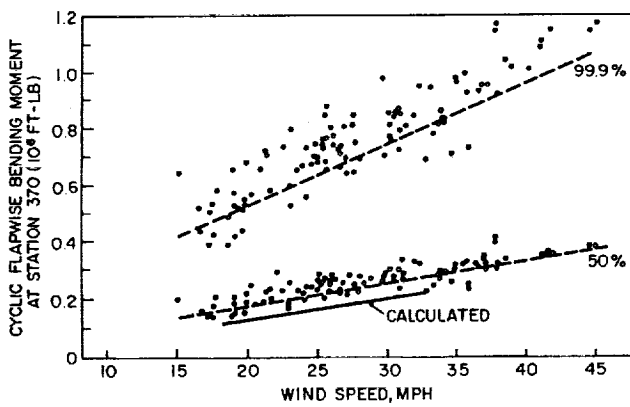370. Data from Reference [3].

Figure B-1. Wind Turbine in Yaw.

Figure 4. Cyclic Flapwise Bending Moment at Station
370. Data from Reference [3]. Calculated
Cyclic Bending Moment is $\frac{1}{2}(M_{max} - M_{min})$.

46